

# Limit Order Book Event Stream Prediction with Diffusion Model

Zetao Zheng<sup>†</sup> Guoan Li<sup>†</sup> Deqiang Ouyang<sup>‡</sup> Decui Liang<sup>†</sup> Jie Shao<sup>†</sup>

<sup>†</sup>University of Electronic Science and Technology of China, Chengdu, China

<sup>‡</sup>Chongqing University, Chongqing, China

{ztzheng, dcliang, shaojie}@uestc.edu.cn liguohan@std.uestc.edu.cn deqiangouyang@cqu.edu.cn

*Abstract*—Limit order book (LOB) is a dynamic, event-driven system that records real-time market demand and supply for a financial asset in a stream flow. Event stream prediction in LOB refers to forecasting both the timing and the type of events. The challenge lies in modeling the time-event distribution to capture the interdependence between time and event type, which has traditionally relied on stochastic point processes. However, modeling complex market dynamics using stochastic processes, e.g., Hawke stochastic process, can be simplistic and struggle to capture the evolution of market dynamics. In this study, we present LOBDIF (LOB event stream prediction with diffusion model), which offers a new paradigm for event stream prediction within the LOB system. LOBDIF learns the complex time-event distribution by leveraging a diffusion model, which decomposes the time-event distribution into sequential steps, with each step represented by a Gaussian distribution. Additionally, we propose a denoising network and a skip-step sampling strategy. The former facilitates effective learning of time-event interdependence, while the latter accelerates the sampling process during inference. By introducing a diffusion model, our approach breaks away from traditional modeling paradigms, offering novel insights and providing an effective and efficient solution for learning the time-event distribution in order streams within the LOB system. Extensive experiments using real-world data from the limit order books of three widely traded assets confirm that LOBDIF significantly outperforms current state-of-the-art methods.

*Index Terms*—event stream modeling, limit order book, diffusion model.

## I. INTRODUCTION

Most modern financial markets use the continuous double auction (CDA) mechanism to determine asset prices. Buyers and sellers interact through physical or digital venues by submitting bid orders (i.e., buy orders) and ask orders (i.e., sell orders), which include price and volume details, into a queuing system known as the limit order book (LOB). A matching engine then pairs these orders into transactions, and the resulting sequence of transaction prices defines the asset’s price at the micro level. Such order data can be effectively represented as an irregularly sampled time series of event stream generated by market participants, along with an event-driven, continuously updated LOB that stores all unexecuted orders in the market. The accumulation of these order streams drives the evolution of the LOB system. Thus, understanding the dynamics of order flow and stream patterns can enhance our ability to predict LOB behavior, providing valuable insights into market depth and potential price movements.

Modeling the event stream LOB presents significant challenges due to its diverse event types, such as order submissions and cancellations on both bid and ask sides, as well as its irregularity, with asynchronous trading actions occurring at arbitrary time points by market participants. A common approach to capturing the arrival of events in LOB is through stochastic point processes, where intensity functions control the frequency of event occurrences over a given time interval. In a naive setting, intensity rates may be independent of past events, as in a Poisson process [1], whereas more sophisticated and realistic models incorporate history-dependent intensity rates, such as in Hawkes processes [2]. Leveraging recent advancements in deep learning, neural point processes have been introduced to model stochastic point processes using neural networks [3], [4]. This integration enhances the predictive accuracy of traditional stochastic models and has demonstrated its state-of-the-art performance in LOB prediction [5]–[7].

However, current mainstream approaches for modeling LOB event stream often rely on specific stochastic point processes [6], [7]. These methods predict event types based on intensity functions learned from event histories. Despite their popularity, they face the following challenges:

- 1) **Simplistic distributional assumptions:** The evolution of the LOB system is highly complex, and using a straightforward stochastic point process (e.g., Poisson process or Hawkes process) often falls short in capturing this complexity. For instance, the Hawkes process models LOB dynamics through intensity functions and decaying functions. However, this simplistic mechanism may struggle to capture the complex dynamics and the continuously evolving nature of the LOB system.
- 2) **Entangled time-event joint distribution:** The time-event joint distribution captures the interdependence between various event occurrence time and types. Modeling these joint time-event distributions for the event stream generally involves a high-dimensional sample space, which makes it highly intractable in practice.
- 3) **Limited support for closed-form sampling:** Many stochastic models, including the ones based on intensity functions, do not easily support closed-form sampling, which refers to the ability to directly sample from a distribution using a deterministic formula without iterative procedures. This limitation hinders efficient and scalable

prediction, especially when dealing with large-scale LOB data streams, where speed and accuracy are crucial.

Addressing the above challenges requires a new paradigm for modeling LOB event stream. To this end, this work proposes LOBDIF (**LOB** event stream prediction with **diffusion** model), a diffusion-based model for event stream prediction in the LOB system, which learns the complex time-event distribution by decomposing it into a Markov chain of multiple steps. Each step represents a small distributional change that can be accurately modeled by a Gaussian distribution [8]. The target distribution is learned through the aggregation of all steps, with the predicted joint distribution from the previous step serving as the condition for the subsequent step. This structure enables closed-form sampling, as each step involves direct sampling from a Gaussian distribution without requiring iterative approximations, making the sampling process both efficient and tractable. By breaking down the complex learning process into a sequence of simpler steps involving Gaussian distributions, LOBDIF captures the evolution of the event stream more accurately and makes the intractable time-event joint distribution more manageable, effectively addressing the challenges faced by previous methods.

However, introducing a diffusion model in LOB modeling presents two significant technical challenges: (1) **Ineffectiveness in modeling time-event relationships**. Capturing the relationship between events at each step of the diffusion process is crucial, as it directly impacts the effectiveness of the final time-event distribution. To address this, a denoising network is designed to capture relationships between time and events. Specifically, time attention and event attention are learned simultaneously to adaptively capture fine-grained interactions, characterizing the underlying mechanisms of the joint distribution. (2) **Low sampling efficiency**. In real-world LOB systems, events occur at high frequency, often requiring rapid decision-making. However, the diffusion model relies on an iterative denoising process to generate samples, which is inherently slow and inefficient for LOB applications. To address this, a skip-step sampling strategy is introduced, which skips some denoising steps during the reverse denoising process, effectively reducing the number of iterations required. This strategy allows for faster sampling without compromising prediction accuracy, significantly enhancing sampling efficiency and making it more suitable for real-time LOB applications.

This paper presents the first systematic attempt to utilize diffusion model in LOB system event stream prediction. The main contributions are three-fold:

- We propose a new paradigm for modeling the event stream in LOB to address the common challenges faced by previous approaches that rely on specific stochastic point processes.
- A denoising network and a skip-step sampling strategy are introduced. The former facilitates learning the time-event joint distribution, while the latter ensures efficient sampling during the denoising phase.
- Experiments on three real-world market datasets demonstrate our model’s effectiveness and efficiency.

## II. RELATED WORK

### A. Modeling of LOB Event Stream

Traditional models for modeling LOB event stream dynamics can be broadly categorized into *stochastic models* and *equilibrium models*. Stochastic models are widely used to capture the probabilistic nature of order stream, typically assuming that events such as the arrival and cancellation of limit orders follow specific probabilistic processes. Some studies model LOB evolution as a higher-order Markov system, where events follow a defined probabilistic structure [1], [9], [10]. For instance, Cont et al. [1] introduced a continuous-time stochastic model that presumes events such as order arrivals and cancellations follow independent Poisson processes, conditioned on the LOB’s current state. Toke and Pomponio [10] shown that a simple bivariate Hawkes process fits nicely their empirical observations of trades-through in limit order book. Additionally, Vvedenskaya et al. [11] formulated LOB dynamics as a discrete-time Markov process governed by nonlinear ordinary differential equations (ODEs). These stochastic models assume that the LOB event stream follows strong probabilistic assumptions, but they may fail to capture the evolution of the event stream due to the variability in high-frequency markets. In comparison, equilibrium models take a game-theoretic approach, focusing on trader interactions and strategic behavior. These models use subjective utility functions to represent payoffs associated with different trading strategies [12], [13]. A prominent variant within equilibrium models is the agent-based model (ABM) [14], where heterogeneous agents with distinct behavior patterns interact within the LOB environment. These methods struggle in highly noisy environments due to the complexity introduced by agent parameters.

In recent years, deep learning has emerged as a powerful tool for modeling and exploiting the dynamics of LOB. Shi and Cartledge [6] combined stochastic point processes with neural networks to model event stream patterns and proposed PCT-LSTM, a state-dependent parallel neural Hawkes process for predicting LOB events. Additionally, they also explored the application of several neural network-based point processes to LOB event stream prediction, such as self-attentive Hawkes process (SAHP) [4] and continuous-time LSTM (CT-LSTM) [3]. Other studies, such as DeepLOB [15], have further explored feature engineering for LOB data, using LOB dynamics to predict price trends. Generative adversarial networks (GANs) have been used to replicate latent patterns within real order stream data [16]. Another work, called stockGAN, employed GANs to generate realistic order streams that capture several stylized facts observed in LOB data [17]. The LOB recreation model (LOBRM) introduced by [18], [19] employed continuous recurrent neural networks to predict volume information at deeper price levels based on trade and quote data.

**Discussion.** The traditional approaches to modeling LOB event stream often restrict it to specific stochastic processes or lack support for advanced networks, limiting their effec-

TABLE I  
COMPARISON OF THE PROPOSED MODEL WITH OTHER LOB MODELING APPROACHES IN TERMS OF KEY PROPERTIES.

Model	No Restr. <sup>(1)</sup>	No Asmp. <sup>(2)</sup>	Flexible <sup>(3)</sup>	Closed-form Sampling <sup>(4)</sup>
Poisson [1]	✗	✗	✗	✓
Hawkes [10]	✗	✓	✗	✗
ODEs [11]	✓	✓	✗	✓
LOBRM [19]	✓	✓	✗	✗
ABM [14]	✓	✓	✓	✗
Stock-GAN [17]	✓	✓	✓	✗
GANs [16]	✓	✓	✓	✗
DeepLOB [15]	✓	✓	✓	✗
PCT-LSTM [6]	✗	✓	✓	✗
<b>LOBDIF (ours)</b>	✓	✓	✓	✓

(1) Without restriction on specific stochastic process.

(2) Without temporal dependence assumption.

(3) Any advanced network architecture can be utilized during the computation.

(4) Sampling without any approximation.

tiveness in capturing the market’s complex dynamics. Agent-based models and recent deep learning-based methods, which use multiple agents to simulate interactions among market participants or employ advanced neural networks, improve the ability to capture event stream dynamics. However, they are unable to achieve closed-form sampling, which introduces challenges in forecasting LOB event stream. In Table I, we present a comparison of different methods for event stream modeling to more clearly highlight their distinctions.

### B. Diffusion Model

Diffusion models have recently emerged as a powerful generative modeling approach, demonstrating success across diverse application domains, including image generation [20], [21], time series prediction and imputation [22]–[26], and data synthesis [27], [28]. Here, the related work focuses on the application of diffusion models to time series tasks, as LOB is essentially a time series problem. These diffusion-based models have demonstrated significant potential in various time series tasks, including forecasting, generation, and imputation. Their ability to capture complex spatio-temporal distribution and handle uncertainty makes them well-suited for both univariate and multivariate time series data.

Diffusion models are increasingly being applied to time series forecasting, particularly for capturing stochastic properties within the data. For instance, D-Va [23] combined deep hierarchical variational autoencoders (VAE) with diffusion probabilistic methods to model stock price volatility, leading to improved forecasting performance. Similarly, TimeDiff [22] incorporated innovations such as future mixup and autoregressive initialization, enhancing the model’s ability to capture intricate sequential patterns and improve forecasting accuracy. In generative tasks, diffusion models have proven valuable for time series applications. DOSE [29] integrated diffusion models with speech enhancement, providing a model-agnostic approach that conditions the diffusion process with additional context to generate clearer speech signals. Disffsformer [30] proposed a conditional diffusion Transformer framework for stock forecasting, which augments time-series stock data with label and industry information. This demonstrates the potential

of diffusion models in data generation tasks beyond traditional predictive applications. Additionally, diffusion models have been applied to imputing missing values in time series data. PriSTI [24] used a conditional feature extraction module based on linear interpolation to handle missing data in spatio-temporal scenarios, while ImDiffusion [25] focused on multivariate time series anomaly detection, applying a conditional weight-incremental diffusion model to enhance imputation and identify anomalies in time series data.

Although diffusion models have shown impressive performance across various fields, their application in modeling the LOB event stream remains relatively unexplored. This work explores the application of diffusion models to LOB event stream prediction for the first time, aiming to extend their applicability to this domain.

## III. PRELIMINARIES

### A. Limit Order Book

Nearly all financial markets operate on the continuous double auction mechanism [31]. Traders submit orders specifying the maximum price they are willing to pay for a specified quantity of an asset, or the minimum price they are willing to accept to sell a quantity of the asset. An LOB is a central component of modern financial markets that records submitted but unexecuted orders. It provides a real-time, dynamic record of all outstanding buy and sell orders at various price levels, effectively serving as a mechanism for matching buy and sell orders. The LOB is organized into two parts:

- Bid side: The buy orders, representing participants willing to purchase the asset at various prices.
- Ask side: The sell orders, where participants offer the asset for sale at different price levels.

Figure 1 presents a schematic of an LOB with 4 price levels evolving over time. Initially, the best bid is at a price of \$99 with a volume of 200, and the best ask is at a price of \$100 with a volume of 100. The next event (at time  $t_1$ ) is a new bid (buy) order at a price of \$100 with a volume of 100. This order executes in full against the best ask, which causes the best ask price to rise to \$101 (the second-best ask price has now become the best bid price). The following event (at time  $t_2$ ) is another bid at a price of \$100 and a volume of 100. However, this ask price is too low to execute (since the current lowest ask is \$101), so the bid order remains unexecuted and is recorded in the LOB on the bid side at the best bid price. As the LOB provides the most detailed demand and supply information available in the market, it is considered the ultimate microscopic level of market structure [32]. The event stream within the LOB is closely tied to its evolution, making the prediction of event streams crucial for understanding the microscopic dynamics of the market.

**Event stream prediction:** Consider an event sequence  $\mathbf{S} = \{(t_1, e_1), \dots, (t_T, e_T)\}$ , where  $t_i \in \mathbb{R}^+$  represents the time and  $e_i \in \{0, 1, 2, 3\}$  represents the event type of the  $i$ -th arrival in the sequence. Event arrivals are categorized into four classes: submission of an order at the bid side

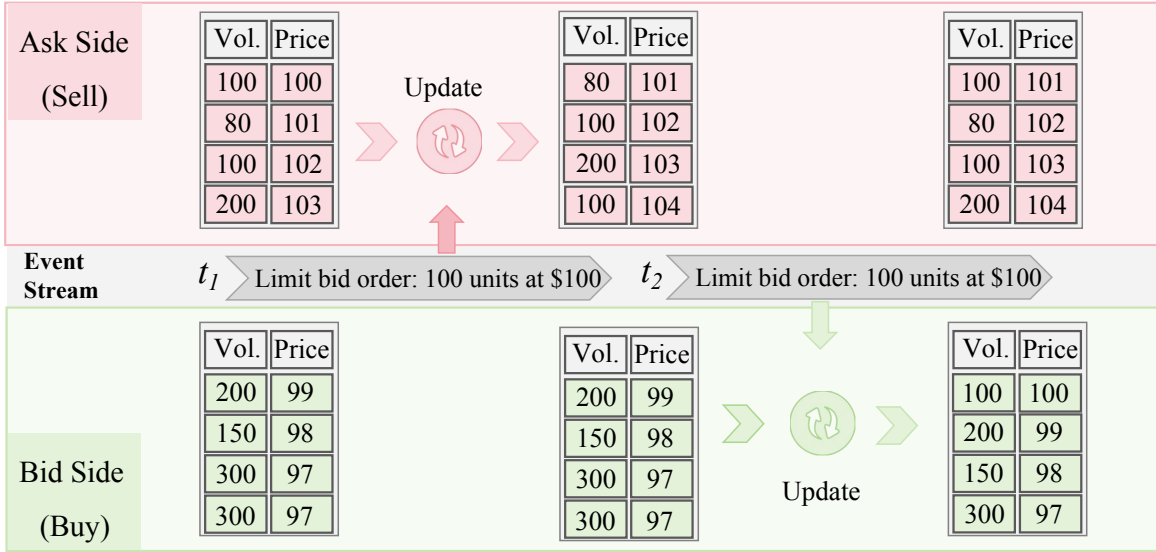


Fig. 1. An LOB with four price levels evolving over time. The event at  $t_1$  matches an order on the ask side, resulting in a successful transaction, while the event at  $t_2$  cannot find a suitable matching price on the ask side and is instead recorded on the bid side.

( $e = 0$ ), cancellation of an order at the bid side ( $e = 1$ ), submission of an order at the ask side ( $e = 2$ ), and cancellation of an order at the ask side ( $e = 3$ ). The event stream  $\mathbf{S}$  is manually divided into equal-length  $L$ -sized sub-streams using a rolling window approach with a step size of one, denoted as  $\{\mathbf{X}_1, \mathbf{X}_2, \dots, \mathbf{X}_{T-L+1}\}$ . Given a sub-stream  $\mathbf{X}_{j \in \{1, \dots, T-L+1\}} = \{\mathbf{x}_1, \dots, \mathbf{x}_L\} = \{(t_1, e_1), \dots, (t_L, e_L)\}$  of length  $L$ , the model receives this event sub-stream as input and makes a prediction for the next event's occurrence time  $t_{L+1}$  and event type  $e_{L+1}$ .

### B. Diffusion Model

Inspired by non-equilibrium thermodynamics, the diffusion model defines a Markov chain of forward diffusion steps that gradually add random noise to data, followed by a reverse denoising process that learns to reconstruct the desired data samples from Gaussian noise. Specifically, given a data point sampled from a real data distribution  $\mathbf{x}^0 \sim q(\mathbf{X}_j)$  (the initial noise-free observation), the forward diffusion process incrementally adds small amounts of Gaussian noise  $\{\epsilon^k\}_{k=1}^K$  over  $K$  steps, resulting in a sequence of progressively noisier samples  $\{\mathbf{x}^1, \dots, \mathbf{x}^K\}$ . The noise levels at each forward diffusion step are controlled by a variance schedule  $\{\beta_k \in (0, 1)\}_{k=1}^K$ . Specifically, at step  $k$ , the observation  $\mathbf{x}^k$  can be obtained from the previous observation  $\mathbf{x}^{k-1}$  as follows:  $\mathbf{x}^k = \sqrt{1 - \beta_k} \mathbf{x}^{k-1} + \beta_k \epsilon^k$ , where  $\sqrt{1 - \beta_k} \mathbf{x}^{k-1}$  represents the scaled contribution of the previous observation, and  $\beta_k \epsilon^k$  indicates the degree of added noise. Since  $\mathbf{x}^{k-1}$  can be inferred from  $\mathbf{x}^0$ , the observation  $\mathbf{x}^k$  can be expressed in a closed-form as:  $\mathbf{x}^k = \sqrt{\bar{\alpha}_k} \mathbf{x}^0 + (1 - \bar{\alpha}_k) \epsilon^k$ , where  $\bar{\alpha}_k = \prod_{i=1}^k \alpha_i$  and  $\alpha_k = 1 - \beta_k$ .  $\epsilon^k$  is the sampled Gaussian noise, denoted as  $\epsilon^k \sim \mathcal{N}(0, \mathbf{I})$ . As the step  $k$  increases, the sampled data  $\mathbf{x}^0$  gradually loses its distinguishable features. Eventually, as  $K \rightarrow \infty$ ,  $\mathbf{x}^K$  converges to a Gaussian distribution.

Mathematically, the entire forward diffusion process is defined as follows:

$$\begin{aligned} \mathbf{x}^K &= q(\mathbf{x}^{1:K} | \mathbf{x}^0) = \prod_{k=1}^K q(\mathbf{x}^k | \mathbf{x}^{k-1}), \\ \mathbf{x}^k &= q(\mathbf{x}^k | \mathbf{x}^{k-1}) = \sqrt{1 - \beta_k} \mathbf{x}^{k-1} + \beta_k \epsilon^k \\ &= \sqrt{\bar{\alpha}_k} \mathbf{x}^0 + (1 - \bar{\alpha}_k) \epsilon^k. \end{aligned} \quad (1)$$

Conversely, the reverse denoising process aims to recover  $\mathbf{x}^0$  starting from  $\mathbf{x}^K$ , where  $\mathbf{x}^K \sim \mathcal{N}(0, \mathbf{I})$ . The observation  $\mathbf{x}^0$  can be inferred progressively from  $\mathbf{x}^K$  as follows:

$$\begin{aligned} \mathbf{x}^0 &= p_\theta(\mathbf{x}^{0:K}) = p(\mathbf{x}^K) \prod_{k=1}^K p_\theta(\mathbf{x}^{k-1} | \mathbf{x}^k), \\ \mathbf{x}^{k-1} &= p_\theta(\mathbf{x}^{k-1} | \mathbf{x}^k) \\ &= \mathcal{N}(\mathbf{x}^{k-1}; \frac{1}{\sqrt{\alpha_k}} \left( \mathbf{x}^k - \frac{1 - \alpha_k}{\sqrt{1 - \bar{\alpha}_k}} \epsilon^k \right), \sigma^2) \\ &= \frac{1}{\sqrt{\alpha_k}} \left( \mathbf{x}^k - \frac{1 - \alpha_k}{\sqrt{1 - \bar{\alpha}_k}} \epsilon_\theta(\cdot) \right) + \sigma \epsilon, \epsilon \sim \mathcal{N}(0, \mathbf{I}), \end{aligned} \quad (2)$$

where  $\sigma = \frac{1 - \bar{\alpha}_{k-1}}{1 - \bar{\alpha}_k} \cdot \beta_k$  and  $p_\theta(\mathbf{x}^{k-1} | \mathbf{x}^k)$  is derived from conditional Bayesian inference.  $\epsilon^k$  is unknown during the denoising process and must be estimated by the neural network. The key idea of the denoising process is to use a neural network  $\epsilon_\theta(\cdot)$  parameterized by  $\theta$ , which takes  $\mathbf{x}^k$  and  $k$  as inputs and outputs the estimated noise  $\epsilon^k$ . The neural network  $\epsilon_\theta(\cdot)$  can be effectively optimized with the following simplified mean squared error (MSE) objective [33]:

$$\begin{aligned} \mathcal{L}_k &= \mathbb{E}_{k \sim [1, K], \mathbf{x}^0, \epsilon^k} [\|\epsilon^k - \epsilon_\theta(\mathbf{x}^k, k)\|^2] \\ &= \mathbb{E}_{k \sim [1, K], \mathbf{x}^0, \epsilon^k} [\|\epsilon^k - \epsilon_\theta(\sqrt{\bar{\alpha}_k} \mathbf{x}^0 + \sqrt{1 - \bar{\alpha}_k} \epsilon^k, k)\|^2]. \end{aligned} \quad (3)$$

The objective of the above function is to guide the neural network  $\epsilon_\theta(\cdot)$  in estimating the Gaussian noise added to the

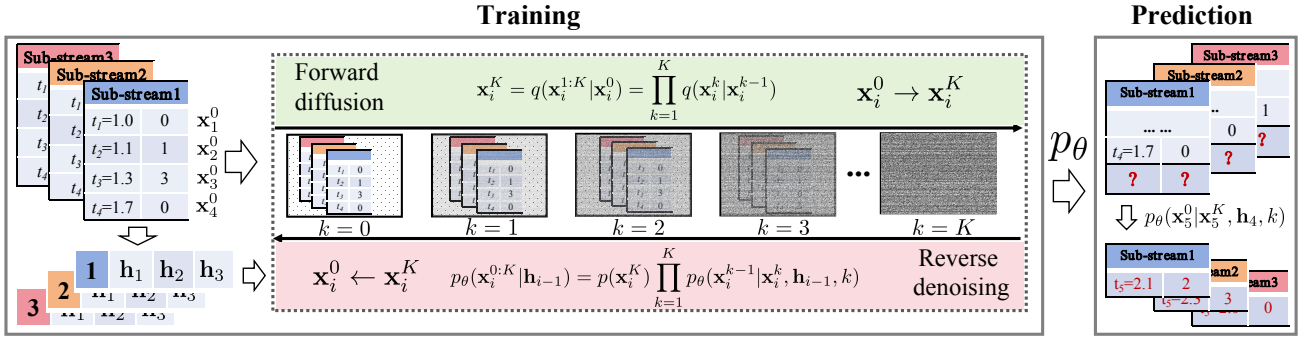


Fig. 2. The overall framework of our proposed method.

input  $\mathbf{x}^k$  and to minimize the error between the actual noise and the predicted noise. Once  $\epsilon_\theta(\cdot)$  can accurately predict the noise, it can transform  $\mathbf{x}^k$  to  $\mathbf{x}^{k-1}$ . This enables the progressive recovery of  $\mathbf{x}^0$  from the initially sampled noise  $\mathbf{x}^K$ .

As described in Eq. (2), each step of the reverse process is explicitly modeled using a deterministic function that incorporates  $\mathbf{x}^k$ , the predicted noise from  $\epsilon_\theta(\cdot)$ , and an additional Gaussian noise  $\epsilon$ . These components enable the diffusion model to inherently support *closed-form sampling*, as it eliminates the need for computationally expensive operations such as Markov chain Monte Carlo or rejection sampling to estimate these variables.

The preliminary information above offers a foundational understanding of the limit order book and diffusion model. Next, we will provide a detailed explanation of how to apply the diffusion model to predict event stream in the limit order book.

#### IV. LOBDIF

Figure 2 illustrates the overall framework of LOBDIF, which consists of a forward diffusion process and a reverse denoising process. In the forward diffusion process, noise is gradually added to the time-event samples. In the reverse denoising process, the noise is progressively removed to recover the original sample. Given the complex relationship between time and event types in LOB event stream prediction, a time-event encoder is employed to better capture the representations of time and event types, along with a carefully designed denoising network that leverages these representations for effective reverse denoising.

##### A. Forward Diffusion Process

For each event  $\mathbf{x}_i^0 = (t_i, e_i)$  in the sub-stream, we model the forward process as a Markov chain. Starting from  $\mathbf{x}_i^0 = (t_i, e_i)$ , we progressively add small amounts of Gaussian noise  $\epsilon_i^1$  to both the time and event components, producing  $\mathbf{x}_i^1$ . This noise-adding process is repeated iteratively until step  $K$  is reached, at which point  $\mathbf{x}_i^0$  evolves into  $\mathbf{x}_i^K$ , resulting in the

sequence  $(\mathbf{x}_i^0, \mathbf{x}_i^1, \dots, \mathbf{x}_i^K)$ . The complete forward process for the event is defined as follows:

$$\begin{aligned} q(\mathbf{x}_i^k | \mathbf{x}_i^{k-1}) &= (q(t_i^k | t_i^{k-1}), q(e_i^k | e_i^{k-1})), \\ t_i^k &= q(t_i^k | t_i^{k-1}) = \sqrt{1 - \beta_k} t_i^{k-1} + \beta_k \epsilon_i^k, \\ e_i^k &= q(e_i^k | e_i^{k-1}) = \sqrt{1 - \beta_k} e_i^{k-1} + \beta_k \epsilon_i^k. \end{aligned} \quad (4)$$

This forward diffusion process is similar to the image-based diffusion models described in Eq. (1), with the key difference being that, while image-based models add Gaussian noise at the pixel level, our approach adds Gaussian noise to the time  $t$  and event type  $e$  in the sampled points.

##### B. Reverse Denoising Process

The reverse denoising process aims to iteratively reconstruct the point  $\mathbf{x}_i^0 = (t_i, e_i)$  from  $\mathbf{x}_i^K \sim \mathcal{N}(0, \mathbf{I})$ . Unlike the image-based denoising process described in Eq. (2), event stream is inherently sequential data. This means that when predicting each step  $\mathbf{x}_i^0$ , we not only rely on  $\mathbf{x}_i^K$  and the step  $k$  as in image-based diffusion models, but also need to account for the historical information prior to  $i$ . Such a setup introduces more complexity, requiring the diffusion model to consider additional dependencies during the denoising process. To account for these dependencies, we encode the previous events,  $\{(t_1, e_1), \dots, (t_{i-1}, e_{i-1})\}$ , into a historical context  $\mathbf{h}_{i-1}$ , which then serves as the condition for predicting the next event  $(t_i, e_i)$ . This can be formulated as follows:

$$\begin{aligned} p_\theta(\mathbf{x}_i^{0:K} | \mathbf{h}_{i-1}) &= p(\mathbf{x}_i^K) \prod_{k=1}^K p_\theta(\mathbf{x}_i^{k-1} | \mathbf{x}_i^k, \mathbf{h}_{i-1}, k), \\ p_\theta(\mathbf{x}_i^{k-1} | \mathbf{x}_i^k, \mathbf{h}_{i-1}, k) &= p_\theta(t_i^{k-1} | t_i^k, e_i^k, \mathbf{h}_{i-1}, k) \cdot \\ & p_\theta(e_i^{k-1} | t_i^k, e_i^k, \mathbf{h}_{i-1}, k), \end{aligned} \quad (5)$$

where  $p(\mathbf{x}_i^K)$  represents sampling a noise from a Gaussian distribution. The key component in the conditional probability function  $p_\theta(\cdot | \cdot)$  is the neural network  $\epsilon_\theta$ , which predicts the noise  $\epsilon_i^k$  based on the current time  $t_i^k$ , event type  $e_i^k$ , denoising step  $k$  and historical context information  $\mathbf{h}_{i-1}$ . With the predicted noise, it becomes possible to derive time and event type predictions according to Eq. (2). This approach allows us to decompose the modeling of the joint time-event distribution into conditionally independent components, which

facilitates more effective modeling of the observed time-event distribution.

Next, we will explain how to obtain the historical context  $\mathbf{h}_{i-1}$  through time-event encoding and how to design the denoising network to compute the previous time  $t_i^{k-1}$  and event type  $e_i^{k-1}$  through denoising network.

1) *Time-event Encoding*: Given the irregular arrival time of events and the discrete nature of their types, we need to effectively represent both time and event types to facilitate capturing the underlying patterns in the order stream. For the time representation, we use a positional encoding method, which encodes time as a continuous representation, as described in Eq. (6). This approach is well-suited for our context because it allows the model to learn relative time relationships between events.

$$\phi(t)[j] = \begin{cases} \cos\left(\frac{t}{10000} \frac{j-1}{M}\right) & \text{if } j \text{ is odd} \\ \sin\left(\frac{t}{10000} \frac{j-1}{M}\right) & \text{if } j \text{ is even} \end{cases}, \quad (6)$$

where  $\phi(t)$  denotes the temporal embedding and  $M$  is the embedding dimension. For the event type, we first encode it as a one-hot vector. To obtain a more expressive representation, we then apply a linear transformation to the one-hot vector to obtain a continuous representation  $\phi(e)$  with  $M$  dimensions. In this way, both time and event types are represented as continuous vectors with the same dimensionality.

For each event  $\mathbf{x} = (t, e)$ , we obtain the event-temporal embedding  $\phi(t, e)$  by adding the time encoding  $\phi(t)$  and the event embedding  $\phi(e)$  element-wise. The embedding for the entire event sequence  $\mathbf{X} = \{(t_i, e_i)\}_{i=1}^L$  is then represented as  $\Phi(t, e) = \{\phi_1, \phi_2, \dots, \phi_L\} \in \mathbb{R}^{L \times M}$ , where each  $\phi_i = \{\phi(t, e)_i\}$ . Additionally, we maintain the separate temporal embedding  $\Phi(t) = \{\phi(t)_1, \phi(t)_2, \dots, \phi(t)_L\}$  and event embedding  $\Phi(e) = \{\phi(e)_1, \phi(e)_2, \dots, \phi(e)_L\}$ . These embeddings are designed to capture distinct characteristics of the temporal and event aspects, allowing the model to adaptively leverage these representations for improved performance.

After the initial event embedding and temporal encoding layers, we pass  $\Phi(t, e)$ ,  $\Phi(t)$  and  $\Phi(e)$  through three self-attention modules. Specifically, the scaled dot-product attention [34] is defined as:

$$\text{Attention}(Q, K, V) = \text{Softmax}\left(\frac{QK^T}{\sqrt{d}}\right), \quad (7)$$

$$S = \text{Attention}(Q, K, V)V,$$

where  $Q$ ,  $K$ , and  $V$  represent the queries, keys, and values, respectively. Taking  $\Phi(t, e)$  as an example, the self-attention operation first takes the embedding  $\Phi(t, e)$  as input, which is then transformed into three matrices via linear projections:  $Q = \Phi(t, e)W^Q$ ,  $K = \Phi(t, e)W^K$ ,  $V = \Phi(t, e)W^V$ , where  $W^Q$ ,  $W^K$ , and  $W^V$  are the weight matrices for the respective linear projections. Afterward, a position-wise feed-forward network is applied to the attention output  $S$  to produce the hidden representation  $h(t, e)$ . For the other two embeddings,  $\Phi(t)$  and  $\Phi(e)$ , the same self-attention operation is used to

generate the hidden temporal representation  $h(t)$  and event representation  $h(e)$ . The final time-event representation of sequence  $\mathbf{X}$ , denoted as  $\mathbf{h}$ , is the concatenation of these three representations, i.e.,  $\mathbf{h} = [h(t, e) \parallel h(t) \parallel h(e)] \in \mathbb{R}^{L \times (3 \times M)}$ . Additionally,  $\mathbf{h}_{i-1}$  refers to the representation at the  $i-1$  position of  $\mathbf{h}$ .

2) *Denoising Network*: We design a denoising network to capture the interdependence between time and event, which facilitates the learning of time-event joint distributions. Specifically, it performs time and event attentions simultaneously at each denoising step to capture fine-grained relations. Each step of the denoising process shares the same structure, which takes in the previously predicted values  $\mathbf{x}_i^{k+1} = (e_i^{k+1}, t_i^{k+1})$ , denoising step  $k$  and the history context representation  $\mathbf{h}_{i-1}$  to achieve conditional denoising. We begin by representing the denoising step  $k$  as a vector to facilitate the model's processing, using Sinusoidal positional embedding [34] to encode  $k$ . Next, we simultaneously compute the time attention  $\omega_t$  and event attention  $\omega_e$  based on the condition  $\mathbf{h}_{i-1}$  and the current denoising step  $k$ . The goal of the time attention and event attention is to generate context vectors by attending to specific parts of the time input and event type input, respectively. The introduction of  $\mathbf{h}_{i-1}$  allows us to account for the dynamic nature of the time-event relationships in the event stream, which impacts the prediction of the next event  $\mathbf{x}_i^0$ . The inclusion of  $k$  considers the dynamics of the diffusion process. These two elements enable the model to adjust its attention based on the evolving dynamics of both time-event relationships and the diffusion process, thereby capturing the complexity of the time-event sequence. The mathematical representation of this process is given as follows:

$$\begin{aligned} \phi_k &= \text{PositionEmb}(k), \\ \omega_t &= \text{Softmax}(f([\mathbf{h}_{i-1} \parallel \phi_k])), \\ \omega_e &= \text{Softmax}(f([\mathbf{h}_{i-1} \parallel \phi_k])), \end{aligned} \quad (8)$$

where  $f$  denotes the feed-forward network and  $\omega_t$  and  $\omega_e$  measure the mutual dependence between time and event. We then combine the historical context of time and event,  $h(t)_{i-1}$  and  $h(e)_{i-1}$ , the previously predicted values  $\mathbf{x}_i^{k+1} = (e_i^{k+1}, t_i^{k+1})$ , along with the denoising step  $k$ , into a feed-forward neural network to model the evolution of time and events. Each layer is formulated as follows:

$$\begin{aligned} \hat{t}_i^k &= \text{ReLU}(f([t_i^{k+1} + h(t)_{i-1} + \phi_k])), \\ \hat{e}_i^k &= \text{ReLU}(f([e_i^{k+1} + h(e)_{i-1} + \phi_k])), \end{aligned} \quad (9)$$

where ReLU denotes the activation function. Finally, the predicted noise is generated by combining time attention, event attention, and the predicted values  $\mathbf{x}_i^k$ , and is given by the following output:

$$\begin{aligned} \hat{\mathbf{x}}_i^k &= [\hat{t}_i^k, \hat{e}_i^k], \\ \epsilon_{t,i}^k &= \sum \omega_t \hat{\mathbf{x}}_i^k, \epsilon_{e,i}^k = \sum \omega_e \hat{\mathbf{x}}_i^k, \end{aligned} \quad (10)$$

where  $\epsilon_{t,i}^k$  and  $\epsilon_{e,i}^k$  are the predicted noise at step  $k$  for the  $i$ -th event. With the predicted noise  $\epsilon_i^k = (\epsilon_{t,i}^k, \epsilon_{e,i}^k)$ , we can optimize  $\theta$  with the true noise  $\epsilon_i^k$  added in the forward process.

---

**Algorithm 1** Training for each event  $\mathbf{x}_i$ 

---

**Require:**  $\mathbf{h}_{i-1}$ 

- 1: **repeat**
- 2:  $\mathbf{x}_i^0 \sim q(\mathbf{X})$
- 3:  $k \sim \text{Uniform}(1, 2, \dots, K)$
- 4:  $\epsilon_i^k \sim \mathcal{N}(0, I)$
- 5: Take gradient descent step on

$$\nabla_{\theta} \|\epsilon_i^k - \epsilon_{\theta}(\sqrt{\alpha_k} \mathbf{x}_i^0 + \sqrt{1 - \alpha_k} \epsilon_i^k, \mathbf{h}_{i-1}, k)\|^2$$

- 6: **until** Converged
- 

In this way, the interdependence between time and event is captured adaptively and dynamically, facilitating the learning of the time-event joint distribution.

## V. TRAINING AND PREDICTION

### A. Training

The training of LOBDIF is based on a similar derivation as in Eq. (3), with the key difference being that the neural network  $\epsilon_{\theta}(\cdot)$  additionally receives the historical context  $\mathbf{h}_{i-1}$ , which accounts for the history of events and their types. The final loss function of LOBDIF is shown as follows:

$$\begin{aligned} \mathcal{L}_k &= \mathbb{E}_{k \sim [1, K], \mathbf{x}_i^0, \epsilon_i^k} \left[ \|\epsilon_i^k - \epsilon_{\theta}(\mathbf{x}_i^k, \mathbf{h}_{i-1}, k)\|^2 \right] \\ &= \mathbb{E}_{k \sim [1, K], \mathbf{x}_i^0, \epsilon_i^k} \left[ \|\epsilon_i^k - \epsilon_{\theta}(\sqrt{\alpha_k} \mathbf{x}_i^0 + \sqrt{1 - \alpha_k} \epsilon_i^k, \mathbf{h}_{i-1}, k)\|^2 \right]. \end{aligned} \quad (11)$$

For each event  $\mathbf{x}_i = (t, e)$  in the sequence  $\mathbf{X}$ , the forward diffusion process will be executed for  $K$  steps, generating  $K$  observations  $\{\mathbf{x}_i^k\}_{k=1}^K$ . Similarly, events in all sequences  $\mathbf{X}_{j \in \{1, \dots, T-L+1\}}$  will undergo the same forward diffusion process, producing a large number of observations. All these observations are included in the training set. The overall framework will be trained in an end-to-end manner. The pseudo-code for the training procedure is shown in Algorithm 1.

### B. Prediction with Skip-step Sampling

To predict the event  $\mathbf{x}_i = (t_i, e_i)$  at timestep  $i$  with a trained LOBDIF, we first obtain the hidden representation  $\mathbf{h}_{i-1}$  by employing the time-event encoder given past  $i$  event sequence. Then, we can predict the next event starting from Gaussian noise  $t_i^K, e_i^K \sim \mathcal{N}(0, I)$  conditioned on  $\mathbf{h}_{i-1}$  based on Eq. (2). However, in practical LOB prediction scenarios, computational efficiency is often strictly required, whereas the reverse denoising process described in Eq. 2 is a time-consuming step-by-step procedure. To make LOBDIF suitable for LOB event stream prediction task, inspired by image-based diffusion models [35], we reformulate  $p_{\theta}(\mathbf{x}^{k-1} | \mathbf{x}^k)$  in Eq. (2) using a reparameterization trick to enable skip-step sampling.

Assuming we start from step  $k$  and skip to step  $s$  (where  $s < k$ ) instead of performing step-by-step denoising, according to Eq. (1), we can define  $\mathbf{x}_i^s$  as Step 1 in Eq. (12).

$$\begin{aligned} \mathbf{x}_i^s &= \sqrt{\alpha_s} \cdot p(\mathbf{x}_i^0 | \mathbf{x}_i^k) + \sqrt{1 - \alpha_s} \epsilon_i^s, \quad \text{Step1} \\ &= \sqrt{\alpha_s} \cdot p(\mathbf{x}_i^0 | \mathbf{x}_i^k) + \sqrt{1 - \alpha_s - \sigma_k^2} \epsilon_{\theta}(\mathbf{x}_i^k, \mathbf{h}_{i-1}, k) + \sigma_k \epsilon, \quad \text{Step2} \end{aligned} \quad (12)$$

---

**Algorithm 2** Predicting  $\mathbf{x}_i^0$ 

---

**Require:** Gaussian noise  $\mathbf{x}_i^K \sim \mathcal{N}(0, I)$  and  $\mathbf{h}_{i-1}$ 

- 1: **Initialize step pairs:**
  - 2:  $\text{pair} = \{(K, K - \tau), (K - \tau, K - 2 * \tau), \dots, (\tau, 0)\}$
  - 3: **for**  $(k, s)$  in  $\text{pair}$  **do**
  - 4:   **if**  $k \geq \tau$  **then**
  - 5:      $\epsilon \sim \mathcal{N}(0, I)$
  - 6:     **else**
  - 7:        $\epsilon = 0$
  - 8:        $\mathbf{x}_i^s = \sqrt{\alpha_s} \cdot p(\mathbf{x}_i^0 | \mathbf{x}_i^k) + \sqrt{1 - \alpha_s - \sigma_k^2} \epsilon_{\theta}(\mathbf{x}_i^k, \mathbf{h}_{i-1}, k) + \sigma_k \epsilon$
  - 9:     **end if**
  - 10: **end for**
  - 11: **return**  $\mathbf{x}_i^0$
- 

where  $p(\mathbf{x}_i^0 | \mathbf{x}_i^k) = \frac{\mathbf{x}_i^k - \sqrt{1 - \alpha_k} \epsilon_{\theta}(\mathbf{x}_i^k, \mathbf{h}_{i-1}, k)}{\sqrt{\alpha_k}}$ , inferred from Eq. (1) and  $\sigma_k = \frac{1 - \alpha_{k-1}}{1 - \alpha_k} \cdot \beta_k$ . We can observe that the equation in Step 1 is unsolvable because it depends on  $\epsilon_i^s$ , whose value is estimated based on  $\mathbf{x}_i^s$ , the very variable we aim to solve. To address this, we apply the reparameterization trick, replacing  $\sqrt{1 - \alpha_s} \epsilon_i^s$  with  $\sqrt{1 - \alpha_s - \sigma_k^2} \epsilon_i^k + \sigma_k \epsilon$ , as described in Step 2. The reparameterization preserves the mean and variance while enabling  $\epsilon_i^s$  to be estimated through  $\mathbf{x}_i^k$  and sampled noise  $\epsilon$ . Note that the initial value of  $k$  is  $K$ , with  $\mathbf{x}_i^K$  being known. Given  $\mathbf{x}_i^K$ , it is possible to progressively derive  $\mathbf{x}_i^s$ , which serves as the starting point for the next skip step.

The skip-step sampling strategy, an extension of the denoising diffusion implicit models [35], [36] from image-based diffusion to the event stream scenario, incorporates sequential attributes such as historical context. A key advantage of this reparameterization is that it eliminates the need for step-by-step sampling, allowing for arbitrary step-size sampling (denoted as  $\tau$ ) without the need of model retraining. The detailed denoising process is outlined in Algorithm 2. This approach significantly enhances the efficiency of the reverse denoising process, as demonstrated in the following example.

**Example 1.** Assuming we progressively add  $K = \{1, \dots, 1000\}$  steps of noise  $\{\epsilon^1, \dots, \epsilon^{1000}\}$  to  $\mathbf{x}^0$  and then train  $\epsilon_{\theta}(\cdot)$  according to Eq. (11). Once  $\epsilon_{\theta}(\cdot)$  is trained, the traditional inference process would first sample the noise  $\mathbf{x}^{1000}$ , then progressively predict the  $\epsilon^k$  value at each step, and obtain  $\mathbf{x}^k$  from  $\mathbf{x}^{1000}$ , eventually reconstructing  $\mathbf{x}^0$ . With skip-step sampling strategy, however, we do not need to follow the entire chain but can instead sample from any subset of steps. For example, we could follow the subset  $\{100, 200, \dots, 900, 1000\}$  rather than the entire chain  $\{1, \dots, 1000\}$ , which enables a  $10 \times$  speed-up in the reverse denoising process.

## VI. EXPERIMENTS

In this section, we conduct experiments to study the following research questions:

- **RQ1:** How does the model's performance compare with existing baseline methods? We present the comparison in Section VI-B.
- **RQ2:** How do the two key components—the time-event encoding and the denoising network—impact model per-

TABLE II  
STATISTICS OF DATASETS.

Datasets	Training events	Valid events	Test events	Types
MSFT-1	343664	42957	42958	4
MSFT-2	303350	37918	37918	4
Pingan-1	77265	14499	14498	3
Pingan-2	53417	9672	9669	3
Telecom-1	80107	15033	15033	3
Telecom-2	65126	10026	10031	3

formance? Additionally, how does the skip-step sampling strategy affect the prediction stage? The results are presented in Section VI-C.

- **RQ3:** How do the key hyperparameters (such as the numbers of forward steps, training epochs, and encoding dimensions) affect the effectiveness of the model? The results are discussed in Section VI-D.
- **RQ4:** How can we gain a better understanding of the reverse denoising diffusion process? The results are presented in Section VI-E.

#### A. Experimental Setup

1) *Datasets:* The six datasets used in our study are sourced from three different markets and time periods. For both MSFT1 and MSFT2, the data are obtained from the NASDAQ market via the LOBSTER platform<sup>1</sup>. We select order data from two different days, dividing each day into 80% for training, 10% for validation, and 10% for testing. The second and third stocks are Pingan Bank from the Shenzhen stock exchange and China Telecommute from the Shanghai stock exchange, both sourced from the CSMAR database<sup>2</sup>. Due to differences in granularity between the two databases, the types of order stream data provided also vary. The LOBSTER dataset includes four types of orders: submit and cancel for both the bid side and the ask side. In contrast, the CSMAR dataset offers only three types of orders: bid, ask, and an unidentified order type. More detailed statistics about the datasets are summarized in Table II.

2) *Evaluation Baselines:* We conduct a comprehensive comparison of the proposed LOBDIF against various state-of-the-art models designed for predicting event arrivals. The evaluation includes five models: (1) Hawkes: A state-dependent stochastic Hawkes point process model with an exponential decaying kernel [37]. This is a stochastic probability-based model that does not rely on neural networks. We implemented it using the open-source library tick<sup>3</sup>, providing a clear contrast to other neural network-based models. (2) LSTM: A straight-forward LSTM-based model that does not include event intensity rate modeling [38], providing a sharp contrast to stochastic probability-based models. (3) CT-LSTM: A neural Hawkes process that utilizes a continuous-time LSTM unit to model

intensity rates for all event types [3]. This model combines the strengths of LSTM and Hawkes processes for event prediction. (4) SAHP: The self-attentive Hawkes process, which replaces the recurrent input structure with an attention mechanism for enhanced representation learning [4]. (5) PCT-LSTM: The state-dependent neural Hawkes process employs stacked CT-LSTM units to separately model the intensity rates for different types of events [6]. This model leverages an enhanced LSTM architecture to simulate event intensities while incorporating the market state for improved prediction accuracy.

3) *Training Setup and Implementation Details:* All experiments are conducted on a machine equipped with an Intel Xeon Silver 4214R CPU, 256GB RAM and an NVIDIA GeForce RTX 3090 (32GB memory). To ensure reliable results and minimize randomness, we run all models five times and average their performance. Our method is compared against several baselines, and their respective results are reproduced using open-source code with optimal settings as described in their respective papers. The proposed LOBDIF is implemented using PyTorch and optimized with the Adam optimizer. During the training phase, we conduct 200 training epochs with a learning rate of  $2.0 \times 10^{-3}$ . The length of the input event history is set to  $L = 50$ , and both the time and event encoding dimensions are set to 64. More details can be found in our code<sup>4</sup>.

For the parameter settings of the comparison models, all linear layers in the LSTM units consist of two layers with 16 units and Tanh activation, whereas the linear layers used to compute the decay coefficient utilize Softplus activation. The attention mechanism in SAHP uses 4 heads. The embedding layers for the event type and state indicator also comprise two layers with 16 units and Tanh activation. The decoding layer for intensity rates consists of a single layer with 16 units and Softplus activation to ensure positive outputs. All models are optimized using RMSprop with a learning rate of  $2 \times 10^{-3}$  and trained for 200 iterations.

4) *Evaluation Metrics:* We evaluate performance using the same metrics as in [6]: (1) Next event time prediction accuracy (denoted as *MAE*), calculated as the absolute difference between the actual and predicted time after applying a common logarithm, which normalizes the wide range of time spans from microseconds to seconds; and (2) Next event type prediction accuracy (denoted as *Acc.*), expressed as a percentage, assessed both when the next event time is known and unknown.

#### B. Comparison Results

The performance comparison is displayed in Table III, where the model with the best performance is denoted in bold and strongest baselines are highlighted with an underline. We observe that neural network-based models outperform the pure stochastic Hawkes model across nearly all evaluation metrics. This is because the stochastic Hawkes model relies on only a few parameters, whereas neural networks can learn

<sup>1</sup><https://lobsterdata.com/info/DataSamples.php>

<sup>2</sup><https://www.csmar.com>

<sup>3</sup><https://x-datainitiative.github.io/tick/index.html>

<sup>4</sup><https://github.com/zhengzetao/LOBDIF>



TABLE III  
PERFORMANCE COMPARISON OF ALL MODELS ON 6 DATASETS.

Datasets	MSFT1		MSFT2		PINGAN1		PINGAN2		TELE1		TELE2	
	Acc.	MAE	Acc.	MAE	Acc.	MAE	Acc.	MAE	Acc.	MAE	Acc.	MAE
Hawkes	0.33	1.72	0.37	1.58	0.36	2.73	0.36	1.99	0.35	2.33	0.37	2.10
LSTM	0.37	-	0.34	-	0.41	-	0.39	-	0.41	-	0.44	-
SAHP	0.40	1.32	0.38	<u>1.01</u>	<u>0.46</u>	<u>2.09</u>	0.45	<u>1.89</u>	0.42	<u>2.14</u>	0.43	1.97
CT-LSTM	0.45	1.11	0.42	1.23	0.37	2.30	0.43	1.96	0.42	2.26	0.44	2.55
PCT-LSTM	<b>0.47</b>	<u>1.07</u>	<u>0.44</u>	1.16	0.38	2.23	<u>0.46</u>	1.91	<u>0.46</u>	2.29	<u>0.45</u>	2.59
LOBDIF	<u>0.46</u>	<b>0.86</b>	<b>0.44</b>	<b>0.84</b>	<b>0.52</b>	<b>1.98</b>	<b>0.50</b>	<b>1.78</b>	<b>0.47</b>	<b>1.96</b>	<b>0.50</b>	<b>1.92</b>
p-value	1.52e-3	4.27e-3	3.05e-3	9.16e-4	6.10e-4	3.05e-3	7.63e-4	4.82e-3	1.68e-3	3.82e-3	7.63e-3	1.53e-3

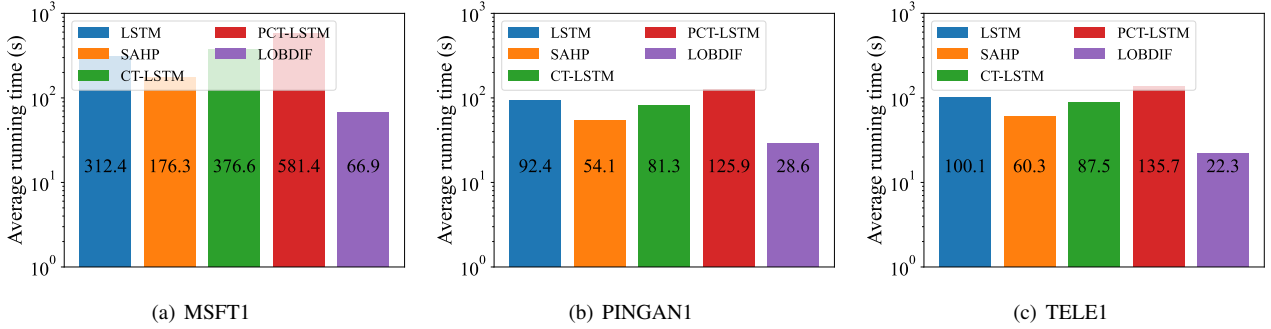


Fig. 3. Average running time comparison for testing dataset execution.

these parameters more effectively, granting the model greater capacity to capture the dynamics of event occurrences. The LSTM model, unlike stochastic point process-based models, treats the event stream as a time series and does not depend on intensity rates. As a result, it cannot predict event time, and only event type prediction results are reported here. Notably, LSTM outperforms the pure stochastic Hawkes model in terms of accuracy, indicating its advantages in event type prediction. The performance improvements achieved by SAHP demonstrate that the self-attention mechanism is more effective for handling long sequences. CT-LSTM and PCT-LSTM both exhibit strong overall performance compared with all other alternatives, with PCT-LSTM performing slightly better, highlighting the advantage of its parallel continuous-time LSTM in handling event types. Our proposed model, LOBDIF, achieves the best overall performance compared with all alternatives, though it is slightly outperformed by PCT-LSTM on MSFT1, still yielding excellent results. This demonstrates that diffusion-based modeling is effective in capturing the complex relationships within the order stream. By decomposing the intricate time-event distribution into multiple Gaussian distributions, the diffusion model facilitates more effective optimization and accurate predictions.

Additionally, we perform the paired Wilcoxon signed-rank test to assess the statistical significance of our method’s performance relative to the strongest baseline. The p-values presented in Table III represent the significance level of the results. The statistical significance analysis is based on 5 pairs of experimental results from our proposed model and

the strongest baseline, with each model being run 5 times using the same parameter settings. A confidence level of 0.05, commonly used in other studies [39], is also applied in our work. If the p-value is less than 0.05, it indicates that the performance of our model is statistically significant compared with the baseline. As shown in Table III, all p-values are below 0.05, confirming that the experimental results are statistically significant and that our proposed model outperforms the baselines.

**Time consumption.** We also compare the average time required to complete testing on the datasets, as shown in Figure 3. For fairness, we exclude the Hawkes model from this comparison, as it cannot be executed on a GPU. It can be observed that our model demonstrates superior efficiency compared with all other models. The average prediction time per step for the three datasets is 1.5 milliseconds, 1.9 milliseconds, and 1.4 milliseconds, respectively (calculated by dividing the total testing time by the number of events). This level of efficiency makes LOBDIF a practical choice for event stream prediction in limit order book. We attribute this outstanding performance to the skip-step sampling mechanism, which significantly enhances the efficiency of the diffusion model. For other models, SAHP exhibits runtime performance second only to LOBDIF, but the LSTM-based models, including CT-LSTM and PCT-LSTM, show inferior efficiency. These models rely heavily on LSTM, which operates as a sequential chain structure, requiring the output of the previous step to compute the next step, leading to inherently slower execution.

TABLE IV  
PERFORMANCE COMPARISON OF LOBDIF WITHOUT TIME AND EVENT ENCODINGS. TE DENOTES THE TIME ENCODING AND EE DENOTES THE EVENT ENCODING.

Datasets	w/o TE		w/o EE		w/o TE & EE	
	Acc.	MAE	Acc.	MAE	Acc.	MAE
MSFT1	-4.1%	-3.4%	-2.3%	-1.9%	-5.1%	-6.4%
MSFT2	-3.6%	-3.4%	-1.9%	-2.3%	-6.4%	-5.5%
PINGAN1	-3.7%	-2.8%	-0.9%	-0.1%	-2.8%	-1.9%
PINGAN2	-3.1%	-3.2%	-1.3%	-0.6%	-3.9%	-3.3%
TELE1	-2.7%	-1.9%	-1.0%	-3.6%	-4.0%	-4.1%
TELE2	-3.2%	-4.5%	-2.1%	-2.6%	-5.3%	-4.7%

### C. Ablation Study

In this section, we conduct ablation studies to investigate the impact of various factors on the model performance. Specifically, we study (1) the influence of the time-event encoder in the denoising process, (2) the impact of the dedicate network in denoising process, and (3) the advantage of skip-step sampling in the prediction phase. We provide detailed explanations of each ablation study in the following.

1) *Influence of Time-event Encoder*: We conduct a detailed analysis of the roles of time encoding and event encoding in the model. The experimental results are presented in Table IV. For clarity, we compare the results of different configurations with the full LOBDIF model results from Table IV and display the differences as percentages. When the time encoding module is removed, the model uses the raw time values concatenated with event encodings as input. Conversely, when the event encoding module is removed, the model uses time encodings along with the one-hot embeddings of events as input. Overall, both modules are indispensable for LOBDIF’s performance. Specifically, time encoding has a more significant impact on the model’s performance, while the effect of event encoding is relatively smaller. This highlights the critical role of time encoding in handling event stream with irregular time point.

2) *Impact of Denoising Network*: To effectively capture the interdependence between time and events, we design a specialized denoising network. To validate its effectiveness, we replace this carefully designed network with MLP and GRU networks, and the experimental results are shown in Table V. Due to space limitations, we present results for only three datasets.

As observed in Table V, our carefully designed network achieves superior performance in both metrics across the three datasets. This is primarily because our network leverages time attention and event attention to effectively capture the interdependence between temporal and event features. In contrast, the other two networks perform poorly. While MLP and GRU can extract either event features or temporal features, their effectiveness is limited to regularly sampled time series. For complex and irregularly sampled time sequences, such as event

TABLE V  
PERFORMANCE COMPARISON OF LOBDIF WITH OTHER DENOISING NETWORKS.

Datasets	MLP		GRU	
	MAE	Acc.	MAE	Acc.
MSFT1	-6.8%	-3.2%	-3.8%	-4.5%
MSFT2	-5.6%	-4.0%	-2.9%	-4.7%
PINGAN1	-7.2%	-5.5%	-4.9%	-6.3%
PINGAN2	-6.7%	-5.1%	-3.2%	-4.6%
TELE1	-5.0%	-3.9%	-2.7%	-4.3%
TELE2	-4.6%	-3.5%	-3.0%	-4.9%

stream in LOB, it is crucial to specifically capture the intricate interdependence between events and time.

3) *Advantage of Skip-step Sampling*: We introduce skip-step sampling to accelerate the denoising process, making it more suitable for LOB event stream prediction scenarios. The model no longer executes a step-by-step denoising process but instead performs skip-step sampling to enhance efficiency, enabling predictions to be completed in fewer steps. In this experiment, we set the number of skipped steps as the parameter  $\tau$ . The parameter  $\tau$  determines how many steps are skipped during the denoising process, thereby influencing the speed of the process. A larger  $\tau$  value means skipping more time steps during denoising, which significantly accelerates the prediction process.

The value of  $\tau$  plays a crucial role in the model’s performance. Under a forward diffusion setup with  $K = 100$  steps, we explore the impact of different  $\tau$  values ( $\tau = \{5, 10, 20, 50\}$ ) with regard to the model’s efficiency and effectiveness. The results, presented in Figure 4, show that as the number of denoising steps decreases, the model’s prediction speed improves significantly. However, this reduction in denoising steps has almost no impact on prediction accuracy, suggesting that the model can maintain performance even with smaller numbers of steps in the denoising process. This indicates that skip-step sampling effectively accelerates the inference process without sacrificing the quality of the predictions. Nevertheless, the speed-up achieved by skip-step sampling is critical for real-time prediction tasks, particularly for large-scale LOB data stream predictions.

### D. Hyperparameter Analysis

Many hyperparameter settings significantly impact the performance of our model. Key factors such as the number of diffusion steps  $K$ , the number of training epochs, and the dimensions of the time-event encoding play critical roles in determining the model’s effectiveness. We analyze the model’s performance under different parameter configurations to discuss optimal parameter selection, with the results shown in Figure 5.

1) *Impact of Diffusion Step  $K$* : The number of diffusion steps,  $K$ , plays a critical role in the model’s performance.

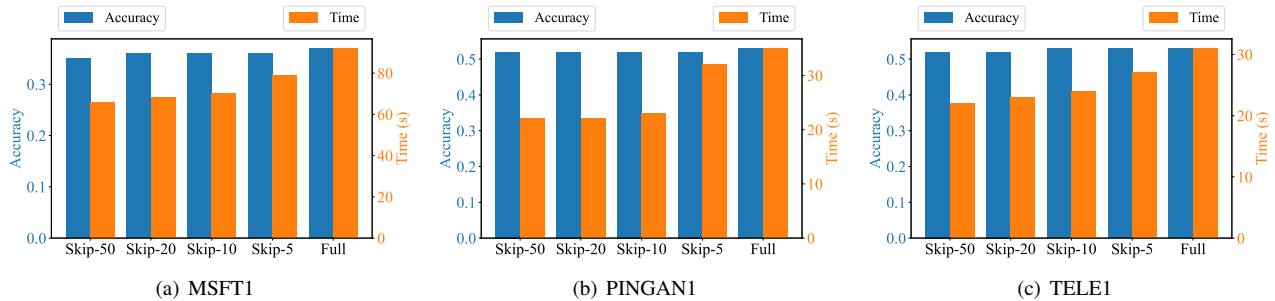


Fig. 4. Average running time comparison for testing dataset execution.

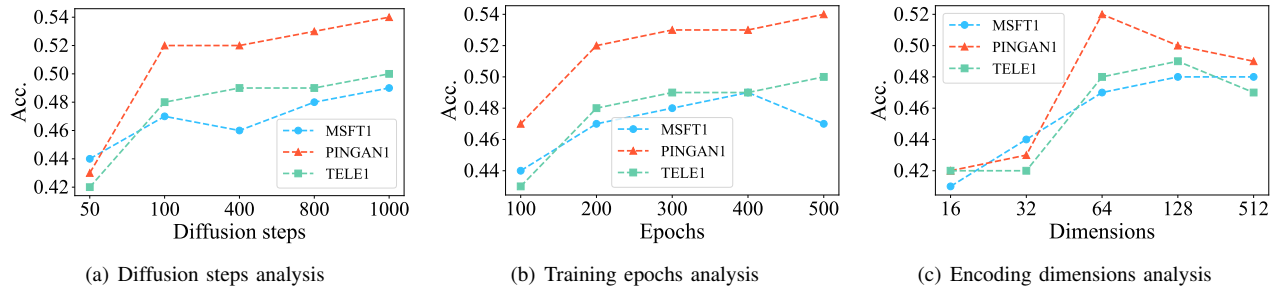


Fig. 5. Analysis of the proposed model's performance with different hyperparameters.

A larger  $K$  allows for a more detailed and granular diffusion process, potentially leading to better predictions. To investigate its impact, we experiment with different values of  $K = \{50, 100, 400, 800, 1000\}$ , analyzing the model's performance and the training time consumption. The results are presented in Figure 5(a). From the figure, we observe that as  $K$  increases, the model's predictive accuracy improves. This improvement occurs because a larger  $K$  enables the model to better approximate the true data distribution, particularly for complex time-event relationships in the event stream. However, this comes at a cost: the training time per epoch increases significantly with  $K$ . This is because each diffusion step involves both the forward pass and the computation of gradients, and a larger  $K$  increases the number of computational steps required during training.

While increasing  $K$  can improve results, there is a diminishing return in accuracy beyond a certain point. For example, the performance gain from  $K = 400$  to  $K = 800$  is much smaller compared with the gain from  $K = 50$  to  $K = 100$ . This indicates that excessively large  $K$  values may lead to diminishing benefits while disproportionately increasing computational cost. Therefore, selecting an appropriate  $K$  value is crucial for balancing model accuracy and efficiency. For practical applications such as real-time predictions in limit order books, a moderate  $K$  may provide the best trade-off between computational feasibility and prediction quality.

2) *Impact of Training Epochs*: We set the model's training epochs to values in the range  $\{100, 200, 300, 400, 500\}$ , with the results illustrated in Figure 5(b). Increasing the number of training epochs generally improves model performance,

as the model is able to better learn the underlying patterns in the data. However, the performance gain becomes less significant beyond a certain point. For example, while the improvement from 100 to 300 epochs is notable, the difference between 400 and 500 epochs is minimal. This suggests that additional training epochs yield diminishing returns once the model approaches its optimal learning capacity.

Moreover, increasing the number of epochs inevitably leads to higher training time consumption. Considering that the forward diffusion process itself is computationally intensive, excessively large epoch values are not practical, especially for time-sensitive applications. Instead, we prioritize a balanced approach, selecting epoch = 200 as an optimal trade-off. This setting achieves good performance without incurring excessive computational cost.

3) *Impact of Encoding Dimension*: We experiment with different encoding dimensions for the model, setting the values to  $\{16, 32, 64, 128, 512\}$ . The results, shown in Figure 5(c), demonstrate how the encoding dimension affects the model's performance. Increasing the encoding dimension generally enhances the vector's representation ability, allowing the model to capture more complex patterns in the data. However, as observed in the figure, the performance improvement becomes less significant as the dimension increases beyond 64. Notably, the model's performance with dimensions of 64 is comparable to that with 256 dimensions. This performance can be attributed to the nature of time and event type data, which do not carry as much complexity or richness as data in other domains, such as natural language or images. Excessively high dimensions may lead to overparameterization, increasing

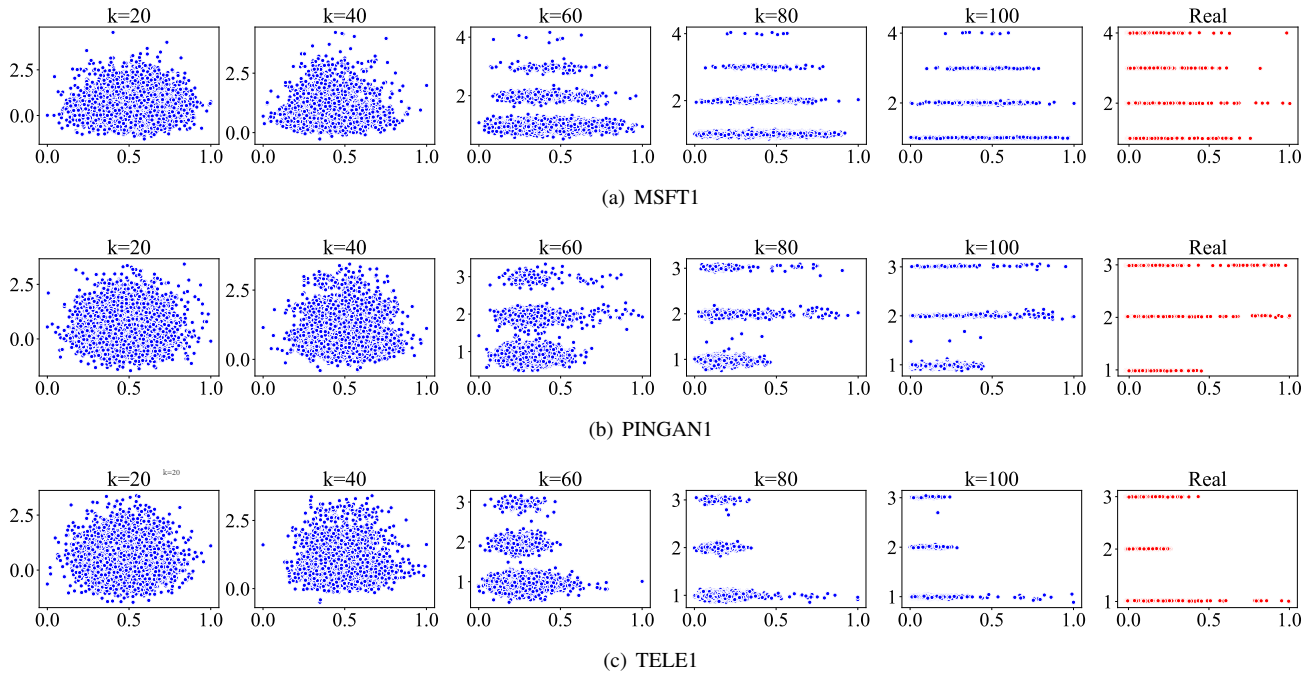


Fig. 6. Visualization of the time-event distribution. The first five columns (in blue) illustrate different stages of the denoising process, while the final column (in red) represents the true time-event distribution. Starting from Gaussian noise, our model gradually approximates the ground-truth distribution

computational costs without meaningful performance gains. For instance, larger dimensions require more memory and longer training time, which are impractical for applications requiring real-time processing. Considering these factors, we select an encoding dimension of 64 as a balanced choice. It provides sufficient expressive power to capture the key patterns in the time and event type data while maintaining computational efficiency.

#### E. Case Study on Denoising Progress

To gain a deeper understanding of the denoising process, we visualize the time-event distribution during the reverse denoising iterations in Figure 6. For better visualization, we normalize the intervals between consecutive timestamps to the range (0, 1). Additionally, only 5000 event points are selected for a clearer representation, with 100 diffusion steps (as a larger number of points would make the visualization too dense).

As shown in Figure 6, at the start of the denoising process, the time-event distribution appears as Gaussian noise. With each progressive denoising iteration, the event type distribution gradually converges towards different event types, while the event time spreads across different time distributions. By the final step, the time-event distribution closely matches the ground-truth distribution, indicating that our LOBDIF model effectively learns the complex time-event relationships.

Moreover, the quality of the denoising improves throughout the iterations, as both the time and event type distributions gradually align with the true distribution. This suggests that the interdependence between the time and event domains is effectively captured in the process of denoising, which

explains the significant improvement in performance during this period.

## VII. CONCLUSION

In this paper, we explore the use of diffusion models for limit order book event stream prediction for the first time. Specifically, we propose a novel model named LOBDIF, which breaks away from the traditional stochastic probability-based prediction methods by leveraging a diffusion model for event stream prediction. The step-by-step mechanism of diffusion models facilitates the decomposition of the complex target time-event distribution into simpler Gaussian distributions, enabling a more effective capture of the interdependence between time and event types. To effectively and efficiently model the relationship between time and event types, we introduce two key components: a denoising network and a skip-step sampling strategy. The denoising network excels at capturing the intricate patterns between time and event types, while the skip-step sampling strategy accelerates the denoising process during prediction, significantly improving efficiency. Extensive experiments demonstrate that our model achieves superior effectiveness and efficiency compared to state-of-the-art methods, validating its potential for limit order book event stream prediction.

## REFERENCES

- [1] R. Cont, S. Stoikov, and R. Talreja, "A stochastic model for order book dynamics," *Oper. Res.*, vol. 58, no. 3, pp. 549–563, 2010.
- [2] F. Abergel and A. Jedidi, "Long-time behavior of a hawkes process-based limit order book," *SIAM J. Financial Math.*, vol. 6, no. 1, pp. 1026–1043, 2015.

- [3] H. Mei and J. Eisner, "The neural hawkes process: A neurally self-modulating multivariate point process," in *Advances in Neural Information Processing Systems 30: Annual Conference on Neural Information Processing Systems 2017*, 2017, pp. 6754–6764.
- [4] Q. Zhang, A. Lipani, Ö. Kirnap, and E. Yilmaz, "Self-attentive hawkes process," in *Proceedings of the 37th International Conference on Machine Learning, ICML 2020*, 2020, pp. 11 183–11 193.
- [5] B. Gasperov and Z. Kostanjcar, "Deep reinforcement learning for market making under a hawkes process-based limit order book model," *CoRR*, vol. abs/2207.09951, 2022.
- [6] Z. Shi and J. Cartledge, "State dependent parallel neural hawkes process for limit order book event stream prediction and simulation," in *KDD '22: The 28th ACM SIGKDD Conference on Knowledge Discovery and Data Mining*, 2022, pp. 1607–1615.
- [7] G. Chung, Y. Lee, and W. C. Kim, "Neural marked hawkes process for limit order book modeling," in *Advances in Knowledge Discovery and Data Mining - 28th Pacific-Asia Conference on Knowledge Discovery and Data Mining, PAKDD 2024, Proceedings, Part III*, 2024, pp. 197–209.
- [8] J. Sohl-Dickstein, E. A. Weiss, N. Maheswaranathan, and S. Ganguli, "Deep unsupervised learning using nonequilibrium thermodynamics," in *Proceedings of the 32nd International Conference on Machine Learning, ICML 2015*, 2015, pp. 2256–2265.
- [9] R. Cont and A. de Larrard, "Price dynamics in a markovian limit order market," *SIAM J. Financial Math.*, vol. 4, no. 1, pp. 1–25, 2013.
- [10] I. M. Toke and F. Pomponio, "Modelling trades-through in a limit order book using hawkes processes," *Economics*, vol. 6, no. 1, pp. 2012–22, 2012.
- [11] N. D. Vvedenskaya, Y. M. Suhov, and V. Belitsky, "A non-linear model of limit order book dynamics," in *2011 IEEE International Symposium on Information Theory Proceedings, ISIT 2011*, 2011, pp. 1260–1262.
- [12] I. Roccu, "A dynamic model of the limit order book," *The Review of Financial Studies*, vol. 22, no. 11, pp. 4601–4641, 2009.
- [13] C. A. Parlour, "Price dynamics in limit order markets," *The Review of Financial Studies*, vol. 11, no. 4, pp. 789–816, 1998.
- [14] F. McGroarty, A. Booth, E. H. Gerding, and V. L. R. Chinthalapati, "High frequency trading strategies, market fragility and price spikes: an agent based model perspective," *Ann. Oper. Res.*, vol. 282, no. 1-2, pp. 217–244, 2019.
- [15] Z. Zhang, S. Zohren, and S. J. Roberts, "Deeplob: Deep convolutional neural networks for limit order books," *IEEE Trans. Signal Process.*, vol. 67, no. 11, pp. 3001–3012, 2019.
- [16] A. Coletta, M. Prata, M. Conti, E. Mercanti, N. Bartolini, A. Moulin, S. Vyetenko, and T. Balch, "Towards realistic market simulations: a generative adversarial networks approach," in *2nd ACM International Conference on AI in Finance, 2021*, 2021, pp. 1–9.
- [17] J. Li, X. Wang, Y. Lin, A. Sinha, and M. P. Wellman, "Generating realistic stock market order streams," in *The Thirty-Fourth AAAI Conference on Artificial Intelligence, AAAI 2020*, 2020, pp. 727–734.
- [18] Z. Shi and J. Cartledge, "The limit order book recreation model (LOBRM): an extended analysis," in *Machine Learning and Knowledge Discovery in Databases. Applied Data Science Track - European Conference, ECML PKDD 2021, Proceedings, Part IV*, 2021, pp. 204–220.
- [19] Z. Shi, Y. Chen, and J. Cartledge, "The LOB recreation model: Predicting the limit order book from TAQ history using an ordinary differential equation recurrent neural network," in *Thirty-Fifth AAAI Conference on Artificial Intelligence, AAAI 2021*, 2021, pp. 548–556.
- [20] R. Rombach, A. Blattmann, D. Lorenz, P. Esser, and B. Ommer, "High-resolution image synthesis with latent diffusion models," in *IEEE/CVF Conference on Computer Vision and Pattern Recognition, CVPR 2022*, 2022, pp. 10 674–10 685.
- [21] Y. Xiao, Z. Huang, Q. Li, X. Lu, and T. Li, "Diffusion pixelation: A game diffusion model of rumor & anti-rumor inspired by image restoration," *IEEE Trans. Knowl. Data Eng.*, vol. 35, no. 5, pp. 4682–4694, 2023.
- [22] L. Shen and J. T. Kwok, "Non-autoregressive conditional diffusion models for time series prediction," in *International Conference on Machine Learning, ICML 2023*, 2023, pp. 31 016–31 029.
- [23] K. J. L. Koa, Y. Ma, R. Ng, and T. Chua, "Diffusion variational autoencoder for tackling stochasticity in multi-step regression stock price prediction," in *Proceedings of the 32nd ACM International Conference on Information and Knowledge Management, CIKM 2023*, 2023, pp. 1087–1096.
- [24] M. Liu, H. Huang, H. Feng, L. Sun, B. Du, and Y. Fu, "Pristi: A conditional diffusion framework for spatiotemporal imputation," in *39th IEEE International Conference on Data Engineering, ICDE 2023*, 2023, pp. 1927–1939.
- [25] Y. Chen, C. Zhang, M. Ma, Y. Liu, R. Ding, B. Li, S. He, S. Rajmohan, Q. Lin, and D. Zhang, "Imdiffusion: Imputed diffusion models for multivariate time series anomaly detection," *Proc. VLDB Endow.*, vol. 17, no. 3, pp. 359–372, 2023.
- [26] D. Liu, Y. Wang, C. Liu, X. Yuan, K. Wang, and C. Yang, "Scope-free global multi-condition-aware industrial missing data imputation framework via diffusion transformer," *IEEE Trans. Knowl. Data Eng.*, vol. 36, no. 11, pp. 6977–6988, 2024.
- [27] H. Cao, C. Tan, Z. Gao, Y. Xu, G. Chen, P. Heng, and S. Z. Li, "A survey on generative diffusion models," *IEEE Trans. Knowl. Data Eng.*, vol. 36, no. 7, pp. 2814–2830, 2024.
- [28] T. Liu, J. Fan, N. Tang, G. Li, and X. Du, "Controllable tabular data synthesis using diffusion models," *Proc. ACM Manag. Data*, vol. 2, no. 1, pp. 28:1–28:29, 2024.
- [29] W. Tai, Y. Lei, F. Zhou, G. Trajcevski, and T. Zhong, "DOSE: diffusion dropout with adaptive prior for speech enhancement," in *Advances in Neural Information Processing Systems, NeurIPS 2023*, 2023.
- [30] Y. Gao, H. Chen, X. Wang, Z. Wang, X. Wang, J. Gao, and B. Ding, "Diffformer: A diffusion transformer on stock factor augmentation," *CoRR*, vol. abs/2402.06656, 2024.
- [31] D. Friedman, *The double auction market: institutions, theories, and evidence*. Routledge, 2018.
- [32] J.-P. Bouchaud, M. Mézard, and M. Potters, "Statistical properties of stock order books: empirical results and models," *Quantitative finance*, vol. 2, no. 4, p. 251, 2002.
- [33] J. Ho, A. Jain, and P. Abbeel, "Denoising diffusion probabilistic models," in *Advances in Neural Information Processing Systems, NeurIPS 2020*, 2020, pp. 6840–6851.
- [34] A. Vaswani, N. Shazeer, N. Parmar, J. Uszkoreit, L. Jones, A. N. Gomez, L. Kaiser, and I. Polosukhin, "Attention is all you need," in *Advances in Neural Information Processing Systems 30: Annual Conference on Neural Information Processing Systems 2017*, 2017, pp. 5998–6008.
- [35] Q. Zhang, M. Tao, and Y. Chen, "gddim: Generalized denoising diffusion implicit models," in *The Eleventh International Conference on Learning Representations, ICLR 2023*, 2023.
- [36] J. Song, C. Meng, and S. Ermon, "Denoising diffusion implicit models," in *9th International Conference on Learning Representations, ICLR 2021*, 2021.
- [37] M. Morariu-Patrichi and M. S. Pakkanen, "State-dependent hawkes processes and their application to limit order book modelling," *Quantitative Finance*, vol. 22, no. 3, pp. 563–583, 2022.
- [38] S. Hochreiter and J. Schmidhuber, "Long short-term memory," *Neural Comput.*, vol. 9, no. 8, pp. 1735–1780, 1997.
- [39] Y. He, X. Chu, and Y. Wang, "Neighbor profile: Bagging nearest neighbors for unsupervised time series mining," in *36th IEEE International Conference on Data Engineering, ICDE 2020*, 2020, pp. 373–384.